Solar gasification of sugarcane bagasse: thermogravimetric analysis of the kinetics of pyrolysis and steam gasification

Master thesis in Chemical Engineering

Elena Cândida dos Santos

April 2012

Advisors: Prof. Maurizio Masi, Prof. Aldo Steinfeld

Chemistry Materials and Chemical Engineering Department "Giulio Natta",
Politecnico di Milano, Milano, Italy

in collaboration with

Institute of Energy Technology
Professorship of Renewable Energy Carriers
ETH – Swiss Federal Institute of Technology Zurich

Acknowledgements

This Master Thesis was written as the requirements for the MSc. degree in Chemical Engineering at Politecnico di Milano - MI.

To Prof. Maurizio Masi, my advisor from my home university, who provided guidance, suggestions and attention.

I would like to cordially thank the ETH Zürich (Swiss Federal Institute of Technology Zurich), represented by Prof. Aldo Steinfeld, who hosted me in the group of Professorship of Renewable Energy Carriers during my entire exchange period.

In special to:

- Michael Krüsi, my supervisor, for lessons, guidance, friendship, encouragement and especially confidence
- Dr. Zoran Jovanovic for having passed his experience, support and friendship.

Special thanks to my mother, Maria Salete dos Santos, for her love, patience and unconditional support in all the moments.

To everyone who contributed directly or indirectly to this work.

Abstract

Solar steam gasification offers an efficient and economic path to provide gaseous, liquid and solid fuels, and prepare chemicals derived from biomass. The thermochemical conversion of the Brazilian sugarcane bagasse in solar-driven gasifiers, can offer an alternative to the sugarcane residue's currently inefficient usage which is the electrical and thermal energy supply for the sugar and ethanol production.

The steam gasification process encloses two consecutive reaction steps: Pyrolysis and steam gasification. Both were experimentally studied by thermogravimetric analysis in order to model their rate laws, which are of fundamental importance for the design of the solar reactor.

Kinetic parameters for pyrolysis and steam gasification have been numerically derived: Pyrolysis reaction is modeled as a linear combination of three-pseudo-components following first order decomposition reactions. The model for the steam gasification reaction is based upon the "oxygen-exchange mechanism" type considering reversible sorption of gaseous species and irreversible reactions among adsorbed species and with molecules from the gas phase. Further, the grain distribution model represented by a linear dependency of the unreacted particles was used to account for the structural changes during reaction.

Keywords: bagasse, pyrolysis, steam gasification, thermogravimetry, steam, kinetics

Table of Contents

1 Introduction

The sugar cane bagasse is a byproduct of the sugarcane industry, as well as sucrose and straw. Bagasse is composed of cellulose, hemicellulose and lignin. Currently the bagasse generated in sugar mills is used to produce energy through co-generation, making the plant self-sustained, and in some cases, spare energy to electricity sales.

In the harvest season 08/09, Brazil processed about 570 million tons of sugarcane, producing around 160 million tons of bagasse. Although it is used as fuel for boilers of the mills, there is left an unused quantity that represents 20% of the total bagasse generation [1]. Hence, there is still a great quantity of bagasse which is incinerated to reduce costs of transportation and treatment. Bagasse is therefore the indicated biomass for further studies and new technologies, such as gasification processes.

At high temperatures and in the presence of steam, bagasse is themochemically converted into syngas. Syngas can be further converted into H_2 via water-gas-shift reaction or to liquid fuels by the well-known Fisher Tropsh reaction, or used directly as combustion fuel to power generation [2, 3]. A schematic of the simplified process can be seen in Figure 1.

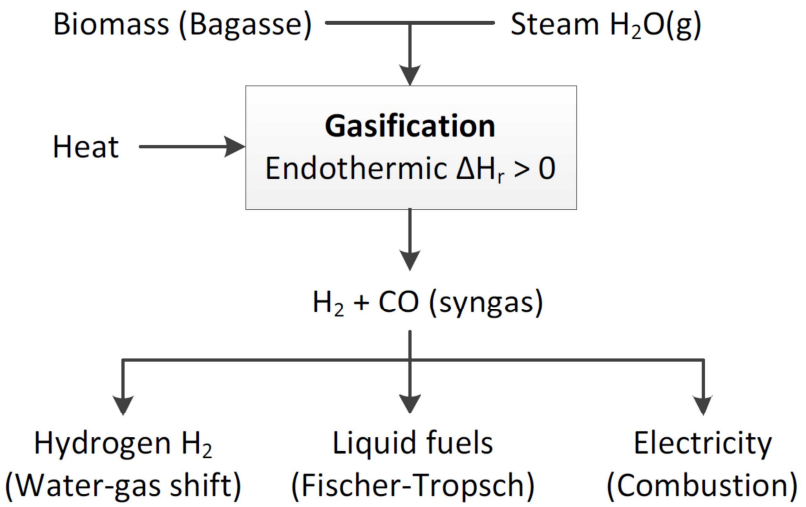

Figure 1: Simplified process diagram

The thermochemical conversion of bagasse occurs via highly endothermic reactions and requires the supply of heat. In the conventional gasifiers, such as autothermal gasifiers, the heat required for the gasification is supplied by the internal combustion of a significant amount of the feedstock with air or pure oxygen [4]. The combustion reduces the utilization of the feedstock and the quality of the syngas due to the increased amounts of CO_2 produced. On the other hand the solar-driven gasification supplies the required heat by concentrated solar energy, which allows working temperatures up to 1500 K [5], moreover, solar energy is chemically stored in the gas product, which leads to a syngas with higher energy content per unit of feedstock and as no combustion occurs, the syngas produced by solar-driven gasifiers has higher quality with lower CO_2/CO and higher H_2/CO ratios. However the challenge of the intermittent solar energy needs to be considered together with the advantages of the solar-driven gasification.

The gasification of biomass is a process that occurs by the combination of two reactions. First, it occurs by the pyrolysis reaction (a thermal decomposition and devolatilization) and subsequently, by the heterogeneous gas-solid reaction of the pyrolysis residue (char) with steam, the so called steam gasification.

Pyrolysis is essentially a devolatilization and decomposition of the organic matter under inert atmosphere leading to the formation of a carbon rich material (char). The nature of pyrolysis is related to the operation conditions. E.g. low or high heating rates applied to pyrolysis may result in different pore structure of char and char yields, which leads to higher or lower reactivity in gasification reactions [6]. The steam gasification is a complex gas-solid reaction of bagasse char with steam because it involves a series of chemical reactions including adsorption and desorption of gases on the solid surface, reactions among adsorbed species, and the release of carbon to gas phase by the formation and desorption of surface oxygen complex.

In the present work, thermogravimetric analyses of pyrolysis and steam gasification were carried out simulating the reactions taking place in the solar gasifier. Kinetic rate laws for both cases were then formulated, as they have a fundamental importance on the understanding and design of the solar reactor.

2 Background

2.1 Conventional gasification

In conventional gasifiers, the heat required for the gasification is supplied by the combustion of a significant amount of feedstock with air or pure oxygen. A simplified rate of reaction for the conventional gasification is expressed in Eq. 1.

$$Biomass + H_2O + \boldsymbol{O_2} \longrightarrow H_2 + CO + \boldsymbol{CO_2} \quad (1)$$

From the heat transfer mode point of view, the conventional gasifiers can be classified as *autothermic* or *allothermic* [5]. In an autothermic process internal combustion of an amount of the solid feedstock with oxygen produces the heat required to run the gasification reaction inside the reactor. In an allothermic process, the heat required is transferred by means of gaseous, liquid (molten salts), or solid heat carrier brought into contact with the reactants or indirectly via heat exchangers.

2.2 Solar driven gasification

In solar driven gasification solar energy is supplied as an external heat source to reach the gasification reaction heat requirement. The solar energy is supplied in form of highly concentrated solar-thermal energy which can reach temperatures up to roughly 1500 K, reported somewhere else [5]. A simplified rate of reaction for the solar driven- gasification is expressed in Eq. 2 as well as a schematic of the process is show in Figure 2.

$$Biomass + H_2O + \boldsymbol{solar\ energy} \longrightarrow H_2 + CO \quad (2)$$

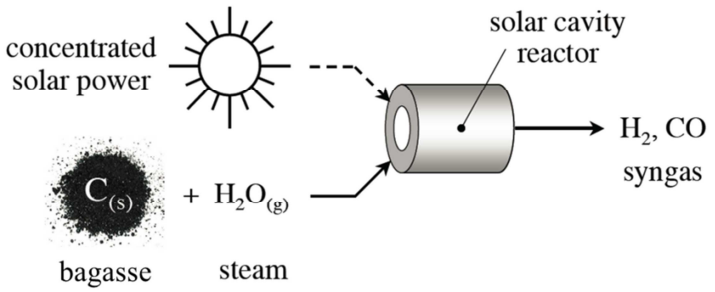

Figure 2: Schematic of the solar-thermals gasification of bagasse

Solar-driven gasification has many advantages compared to the conventional one. As it uses highly concentrated solar-thermal energy to gasify the carbonaceous feedstock, there is no need to combust part of it to produce the heat required by the gasification. Therefore, it does not account for carbon dioxide realize into the atmosphere. Moreover, solar energy is chemically stored in the gas product, which leads to a syngas with higher energy content per unit of feedstock. Since no internal combustion contaminates the syngas, it is of higher quality with lower CO_2/CO and higher H_2/CO ratios. This reduces the effort for separating CO_2 when producing Fischer-Tropsch liquid fuels, reducing investment costs of additional separation units.

These advantages of solar gasifiers over conventional ones are to be considered in combination with the introduced challenges by the intermittent energy of the sun.

Solar gasification reactors may be classified as [5]:

- directly irradiated reactors: where the solid carbonaceous reactants are directly exposed to the concentrated solar irradiation. E.g. a vortex-flow solar reactor featuring a helical flow of carbonaceous particles and steam, where the heat transfer is consider fast, meaning that pyrolysis is conducted with a high heating rate.
- indirectly irradiated reactors: where heat is transferred to the reaction site through an opaque wall. E.g. solar-packed-bed reactor, in which the thermal dissipation is slow, comparable to a slow heating rate.

The present work studies the kinetics involving pyrolysis and steam gasification that take place inside a solar gasifier. This is crucial for the understanding and design of a solar reactor.

3 Pyrolysis

Pyrolysis is a thermal decomposition of carbonaceous materials under inert atmospheric conditions or in a limited supply of air [8], leading to the release of volatiles and formation of a carbon rich solid (char). It is an endothermic process and requires the supply of heat.

Pyrolysis of biomass is typically initiated at 473 K and lasts until 623-723 K depending on the species of biomass. The nature of pyrolysis and the evolving gases are related to the operation conditions, such as particle size, heating rate and temperature.

Their influences are deepened in the following:

- Particle size: it is believed [9] that increasing the particle size will lead to higher devolatilization times.
- Heating rate: influences the volatiles release behavior and may have a significant impact on the reactivity of the char. It is believed [6] that rapid heating rates inhibits secondary reactions and prevents the formation of tars. Moreover the latter produces chars with strongly non-uniform distributed macro-pores leading higher reactivity in gasification.
- Temperature: impacts on the pyrolysis yields and its product properties. Pyrolysis at high temperatures produces mainly gases while the low temperature pyrolysis produces tar and liquid derivatives, such as tar and heavy oils [10].

Depending on the solar reactor design, shown in scetion 2.2, slow or rapid pyrolysis may take place. As explained before, this can lead to chars with different properties, such as pore size and reactivity in gasification. For this reason, in this work both pyrolysis treatments were studied by the steam gasification reaction.

Furthermore, the determination of the kinetic parameters of pyrolysis allows the mathematical modeling of the rate of chemical reactions taking place during the devolatilization of the biomass. The kinetic parameters allow determining the time required for complete conversion of the solid material [11]. Thus, the design of the solar reactor for the thermochemical conversion of biomasses requires also the investigation of the pyrolysis reaction.

3.1 Models of reaction kinetics

Modeling of pyrolysis implies the representation of the chemical and physical phenomena in a mathematical form. The basic equations are those of chemical kinetics, heat transfer and mass transfer. The actual reaction scheme of pyrolysis of biomass is extremely complex because of the formation of more than hundred intermediate products. Despite of the considerable number of research works devoted to the kinetics of biomass pyrolysis, the definition of the right kinetic model remains controversial [7].

As far as empirical modeling concerns, the main proposed kinetic mechanisms are based either on a one step reaction (global decomposition) or on several competitive parallel reactions, where all of them constitute derivations of a summative model for pyrolysis, called *distribution of activation energy model*, originally developed by Pitt [12] and still widely accepted today.

The pyrolysis reaction can be described by means of the following scheme:

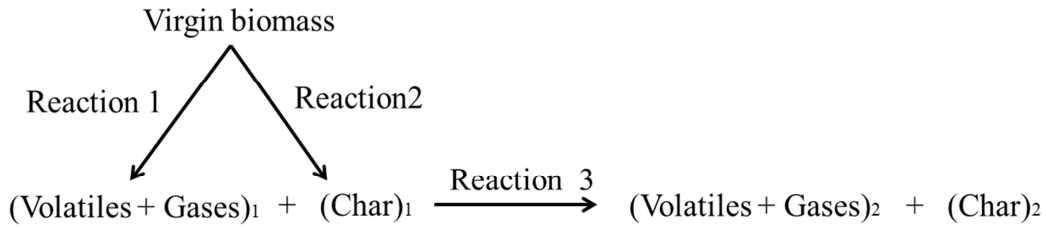

Figure 3: Pyrolysis mechanism

This scheme shown in Figure 3 indicates that the biomass decomposes to volatiles, gases and char. The volatiles and gases may further react with char to produce different type of volatiles, gases and char where the compositions are different. Therefore, the primary pyrolysis products participate in secondary interaction (Reaction 3), resulting in a modified final product distribution.

The present work aims to find a rather simple kinetic model that is suitable to the experiments carried out. Therefore the rate of pyrolysis is calculated as a combination of first-order decomposition rates of pseudo-components. The competitive outlines refer to parallel, irreversible and first order reactions to get the different fractions of pyrolysis products associated with activation energy with a characteristic decomposition temperature.

Based on the above assumptions, the rate of pyrolysis is calculated as:

$$\frac{dX_i}{dt} = k_i'(1 - X_i) \tag{3}$$

where,

$$X_i(T,\ t) = \frac{m_{0,i} - m_i(T,t)}{m_{0,i}} \tag{4}$$

where $m_i(T,t)$ denotes the mass of the pseudo-component i having reacted until temperature T and time t while $m_{0,i}$ is the total initial mass fraction of pseudo-component i. k_i' is assumed to follow Arrhenius law,

$$k_i' = k_{i,0}'\, exp\left(-\frac{E_a}{RT}\right) \tag{5}$$

The temperature rising is expressed as a function of time t, the TG's heating rate HR, and the temperature at the starting point of the heating phase T_0,

$$T(t) = T_0 + HR.t \tag{6}$$

Solving Eq. 3 for X_i gives the conversion of pseudo-component i up to a temperature T considering conversion achieved during the non-isothermal phase of duration t (constant heating).

$$X_i = \left\{1 - exp\left[-\frac{k_{i,0}}{HR}\int_{T_0}^{T} exp\left(-\frac{E_{a,i}}{RT}\right) dT\right]\right\} \tag{7}$$

The total conversion (Eq. 8) and total conversion rate (Eq. 9) of all components of the biomass sample are then calculated as:

$$X_T = \sum_{i=1}^{3} X_i \tag{8}$$

$$\frac{dX_T}{dt} = \sum_{i=1}^{3} k_i'(1 - X_i) \tag{9}$$

According to Orfao et al. [13] the subscripts i do not refer exactly to the natural polymers that integrate the biomass but to the three any pseudo-components.

3.2 Sample preparation and characterization

The bagasse was received directly form a Brazilian sugar mill in the form of particles mixed with long fibers containing still a lot of moisture. Prior to its use, the bagasse was sieved with a 1mm sieve and soon after oven dried for 16 hours at 376 K.

3.2.1 Bagasse characterization

The composition of bagasse, are expressed in terms of proximate and ultimate analyses, which are generally used to characterize solid fuels. Data analyses are shown in Table 1.

Table 1:Ultimate analysis of bagasse (dry basis); C, H, N determined with CHN-900, O with RO-478 and S with CHNS-932 (all LECO Corporation, St. Joseph, MI)

Carbon (C)	[$\%_{wt}$]	42.51
Hydrogen (H)	[$\%_{wt}$]	5.94
Oxygen (O)	[$\%_{wt}$]	37.54
Nitrogen (N)	[$\%_{wt}$]	0.41
Sulfur (S)	[$\%_{wt}$]	0.09
Ash	[$\%_{wt}$]	13.51
H/C = x	[mol/mol]	1.665
O/C = y	[mol/mol]	0.663

Table 2:Proximate analysis of bagasse (dry basis), determined by thermogravimetric analysis (Netzsch STA 409 CD)

Volatiles	[$\%_{wt}$]	77.3
Fixed carbon	[$\%_{wt}$]	12.6
Ash	[$\%_{wt}$]	10.2

A higher heating value (HHV) of 11.56 MJ/kg was determined by calorimetric analysis (Calorimeter C7000, IKA-Werke). The lower heating value (LHV) of 8.97 MJ/kg was calculated based on the HHV and the elemental composition of the bagasse on a moisture free basis. The particle size distribution of the bagasse sample, measured by laser scattering (LA-950 analyzer; HORIBA,) is shown in Figure 4, and indicates a mean particle size of 455 µm. The ultimate analysis revealed an average chemical formula for bagasse of $CH_{1.665}O_{0.663}N_{0.008}S_{0.001}$ on a dry and ash free (d.a.f.) basis. Nitrogen and sulfur were neglected and $CH_{1.665}O_{0.663}$ was assumed to adequately represent the sample.

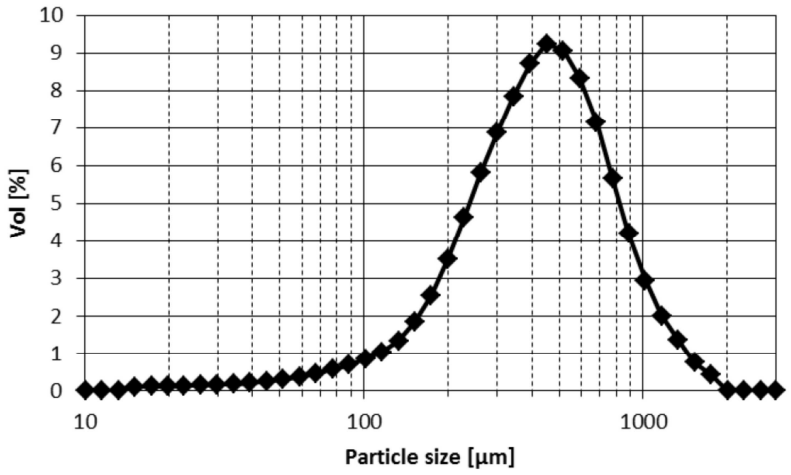

Figure 4: Volume based particle size distribution for bagasse sieved with 1mm sieve.

3.3 Thermogravimetric analysis

The experiments in this chapter were performed with a thermogravimeter system (Netzsch STA 409 CD) equipped with a furnace that is a conventional high-temperature electric furnace (Figure 5) with a maximum working temperature of 1823 K. This furnace is suitable for experiments with controlled reactive gas atmospheres having a dew point below room temperature.

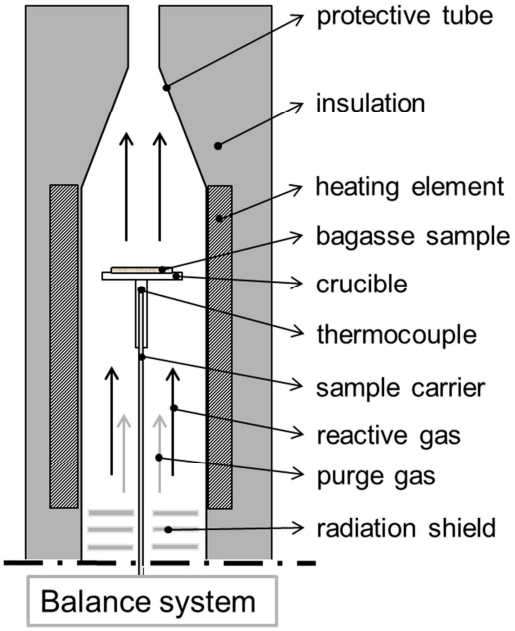

Figure 5: Cross-sectional schematics of the Netzsch high-temperature furnace

The pyrolysis experiments were performed with dish shaped crucibles that are made of aluminum oxide (Al_2O_3) and have an outer diameter of 17 mm. The sample carrier connecting the crucible with the balance is equipped with a thermocouple type S and measures the temperature directly at the sample crucible. Bagasse samples were mounted as a thin layer on the flat sample crucibles and swept by the inert gas flowing through the furnace. This arrangement avoids stagnant gas around the sample and minimizes mass and heat transfer resistances between the bagasse sample and the bulk gas [14, 15].

The measuring part of the STA 409 thermogravimeter features a vacuum proof housing suitable to realize controlled atmospheres such as reactive or inert. The experimental setup

includes a TASC 414 System Controller for temperature programming and data acquisition. The weight signal from the digital balance and the temperature signal from the sample thermocouple are recorded with a nominal accuracy of $5 \cdot 10^{-3}$ mg and 0.1 K, respectively.

This setup has a single furnace wall and features a bottom up flow. The furnace chamber is separated from the balance by means of a ceramic radiation shield, and the gas exit is located at the top end.

The pyrolysis experiments were conducted allowing the investigation of the thermal decomposition over the whole temperature range from room temperature up to 1473 K. A non-isothermal (dynamic) temperature program was used starting at 298 K and ramping up with a linear heating rate, HR = 10 to 30 K/min, to the final pyrolysis temperature of 1473 K. Experiments are performed with inert sample atmospheres consisting of 100% argon at a flow rate of 100 mL_N/min and a total pressure of 1 bar.

An 8 mg bagasse sample, weighed on an external Mettler Toledo XS105 DualRange high precision balance was placed as a thin layer on the flat sample crucible stored in the TG furnace. The furnace chamber was purged for 30 minutes with argon to ensure an inert atmosphere at the beginning of the experiment. Once this is done, the temperature program was started and automatically completed by the control system.

Table 3 presents a list with the pyrolysis runs and the respective temperature and concentration data.

Table 3: Pyrolysis runs in the high temperature furnace with the corresponding experimental parameters.

	m_0 (mg)	T_0/HR/T_{end} (K,K/min,K)	Purge (F_{Ar}) (mL_N/min)	F_{Ar} (mL_N/min)
Bagasse	8.10	298/10/1473	132	100
	8.10	298/20/1473	132	100
	8.06	298/30/1473	132	100

3.4 Results and discussion

The typical TG and DTG (derivative of TG) curves obtained for the slow pyrolysis of bagasse are shown as an example for heating rate of 20 K/min in Figure 6.

The experimental runs were performed with dried particles with a mean particle size of 455 µm, subjected to an argon flow of 100 mL_N/min and a linear heating rate of 10 to 30 K/min in the 298-1473 K temperature interval. According to the kinetic model elaborated, pyrolysis is considered as a linear combination of first order decomposition steps.

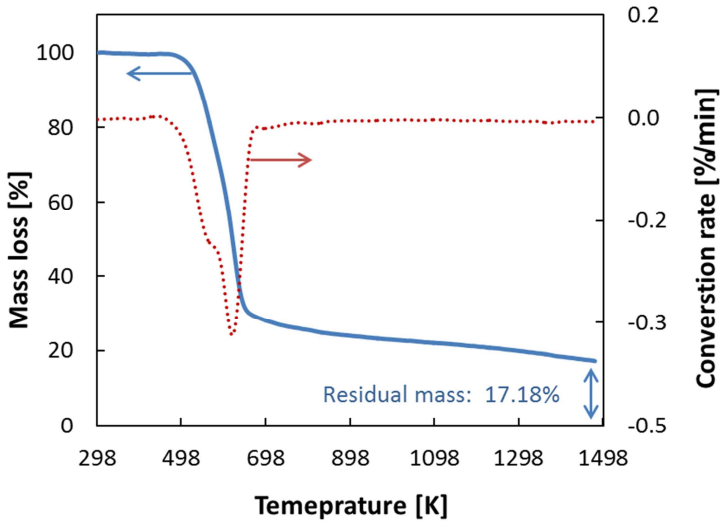

Figure 6: TG and DTG data for the pyrolysis of bagasse at HR = 20 K/min

The complete decomposition of a pseudo-component is characterized by a minimum in the DTG curve. Just by visualizing Figure 6, bagasse pyrolysis could be represented by two steps process. However, as this feedstock is constituted by cellulose, hemicellulose and lignin, at least three pseudo-components should appear in the DTG curve. This, not accounting for the complexes that might be formed between these compounds. Therefore pyrolysis was considered a three-step process.

By varying the heating rate, it was attempted to verify its dependence on the kinetic parameters evaluation. Accordingly to Vargegyi et al.[16], the most suitable way to judge the

reliability of the parameters appears to be a comparison of the parameters obtained from measurements at different heating rates.

The DTG curves of bagasse pyrolysis exhibit a first minimum at 566.6 K, a second, at 601.5 K, and a third at 618.6 K.

The total weight loss during pyrolysis of the bagasse up to 1473 K is around 83%. Figure 6 shows that a residual mass of around 17% is encountered. The latter accounts for the quantity of char and ash.

For modeling the pyrolysis rate of reaction a least square method was used to fit the kinetic parameters. Figure 7 shows the experimentally measured and numerically modeled conversion rate and conversion for a 3-pseudo-component fit applied to the pyrolysis reaction of bagasse with a heating rate of 20 K/min.

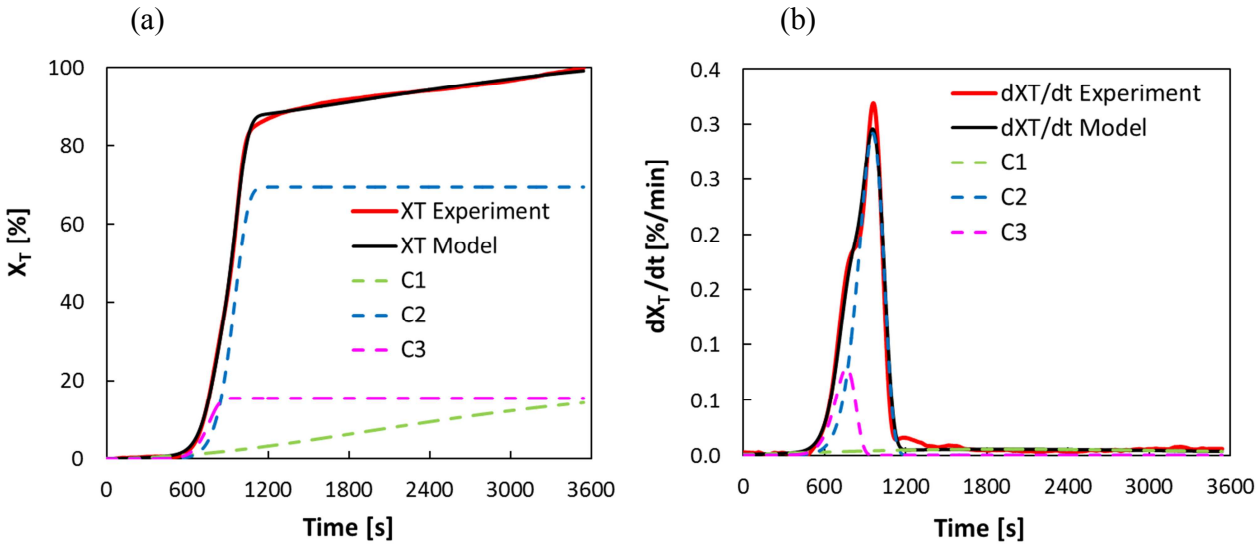

Figure 7: Experimentally measured and modeled 3-pseudo-component conversion (a) and rate of conversion (b) applied to the slow pyrolysis reaction of bagasse.

The accuracy of the fitting is defined as:

$$RMS = \sqrt{\frac{1}{n}\sum_{Y_i}^{n}(Y_i - \overline{Y}_i)^2} \qquad (10)$$

where Y_i is the data measured in the experiments, $\overline{Y}_i$ is the numerically modeled data and n is the number of summations, i,e, number of experimental points

The agreement is reasonably good for the conversion rate and the conversion. The conversion of pseudo-components C2 and C3 replicates satisfactorily their devolatilization reaction in the 423- 698 K rage. However, C1, which was expected to devolatilize at higher temperatures, did not demonstrate the same behavior. As Roque-Diaz et al.[17] speculated in bagasse pyrolysis, for a temperature range of 723-1173 K, the cracking reaction of C-C bonds occurred. The pyrolysis of bagasse should be finished after that, but as one can see from Figure 6, the reaction continued and did not finished up to 1473 K, explaining why the pseudo-component C1 did not fulfill the expectations.

The series of equations, Eqs. 3-9, were used to fit the experimental data of the devolatilization of the pseudo-components measured by TG. From this fits kinetic parameters $k_{0,i}, E_{a,i}$ and X_i were extracted from each of the three pseudo-components as are summarized in Table 4.

Table 4: Arrhenius kinetic parameters for 3-pseudo-component model applied to the pyrolysis of sugar cane bagasse.

HR [K/min]	**Pseudo component : C1**			**Pseudo-component : C2**			**Pseudo-component: C3**		
	X_1 [-]	k_0^1 [s^{-1}]	Ea_1 [J/mol]	X_2 [-]	k_0^2 [s^{-1}]	Ea_2 [J/mol]	X_3 [-]	k_0^3 [s^{-1}]	Ea_3 [J/mol]
10	0.14	8.62E-05	2.33E+04	0.37	1.34E+05	1.02E+05	0.47	8.59E+04	1.03E+05
20	0.18	7.45E-05	1.05E+04	0.68	1.74E+05	1.02E+05	0.17	1.00E+05	8.86E+04
30	0.30	1.82E-05	4.65E+03	0.75	8.06E+04	9.66E+04	0.11	1.15E+05	8.90E+04

The apparent activation energies $E_{a,i}$ found are lower than the ones found by Manya et al. [18], who carried out pyrolysis of bagasse at heating rates of 5 K/min. Nevertheless regarding the same aforementioned author, apparent activation energies tend to be obtained higher at lower heating rates. The decomposition was also found to occur at lower temperatures.

4 Steam gasification

Gasification of lignocellulosic materials, such as sugar cane bagasse with steam, is a heterogeneous gas-solid reaction of char, produced primarily by pyrolysis of the carbonaceous material, and steam. A simplified reaction can be expressed as,

$$C + H_2O \leftrightarrow CO + H_2 \qquad \Delta H_R = 131\ kJ/mol \qquad (11)$$

The net reaction of the steam gasification is strongly endothermic, thus heat needs to be supplied. The product of the reaction is mainly hydrogen and carbon monoxide, the so called syngas or synthesis.

The gasification rate is mainly dependent on temperature and partial pressure of the gaseous reactants. Due to the exponential dependency of temperature, described by the Arrhenius law, the influence of temperature is much more evident than the partial pressure of the reactants.

Even if the partial pressure influence is not very notable it is necessary to care about the concentration and type of the gaseous reactants at the solid surface. Therefore, transport of reactants from the bulk phase to the core of the solid particles and transport of products the way back to bulk phase needs to be accounted.

Moreover it is also strongly dependent on the solid surface available for the gas-solid reaction. As one can imagine the latter reaction may involve complex reactions such as adsorption of the reactant at the solid surface, surface reaction though molecule complexes, and desorption of products.

4.1 Models of reaction kinetics

The modeling of heterogeneous gas-solid chemical reactions is complicated by a series of issues not encountered in homogeneous systems. Since more than one phase is present, rate equations for heterogeneous reactions often incorporate mass transfer terms in addition to the usual chemical kinetic term. The mass transfer terms may differ in type and number depending

on the shape of the heterogeneous system. A general rate expression that holds for all reacting system is not available.

It is evident that the gas-solid reaction taking place on a surface must depend on its chemical adsorption of the fluid reactants. Many features of heterogeneous kinetics of solid-gas reactions have been explained by this hypothesis and the application of Langmuir's adsorption isotherm [19]. For a gas-solid reaction as it is encountered in the steam gasification of bagasse, the following set of consecutive reaction steps can be identified:

Step I Diffusion of the reactant from the bulk gas through the gas film to the external particle surface.

Step II Diffusion of the reactant from the particle surface through the pores to a reaction site.

Step IIIA Reactant adsorbs on the surface and is attached to an active site.

Step IIIB Reaction with the solid or a molecule from the gas phase (single site mechanism) or with an adjacent active site (dual site mechanism).

Step IIIC Desorption of the products from the solid surface.

Step IV Diffusion of the products from the reaction site across the pores to the particle surface.

Step V Diffusion of the products from the external particle surface to the bulk gas.

Steps I and V describe the mass transfer of gaseous reactants and products across the fluid film surrounding the bagasse char particle. The structural particle model in Chapter 4.1.1 considers the steps II and IV. Steps IIIA to IIIC are considered by the oxygen-exchange model and treated in Chapter 4.1.2.

Depending on the physical and chemical boundary conditions of the system such as temperature, pressure, stoichiometry of the reaction, and solid porosity, different steps from the list above can become rate controlling since it is always the slowest step that controls the overall rate of the process. For the measurement chemical, it is desirable to choose the experimental conditions in order to obtain chemical reaction control, which is usually encountered at low temperatures. If this is not feasible diffusion effects have to be considered in the model, leading to undesired complication.

It is essential to have a mathematical model that correctly reproduces the physical situation of the reacting system. A mismatch in the controlled regime for example, can easily result in a situation where the reaction kinetics have been simulated with an amazing degree of accuracy and just the same the resulting equations fail to give a correct prediction of a scale-up [20].

Based on the Arrhenius plots illustrated in Figure 8, three main regimes are introduced in solid conversion: chemical, diffusional and mass transfer regimes. The regime that is controlled by the chemical reaction is established when temperatures are low and char particles are so small that diffusion rate is much faster than chemical reaction. Diffusion effects during char gasification may be important even for conditions of themogravimetric analysis [15].

An assessment of these effects should be done for the entire range of conversion and operating conditions before the kinetic evaluation.

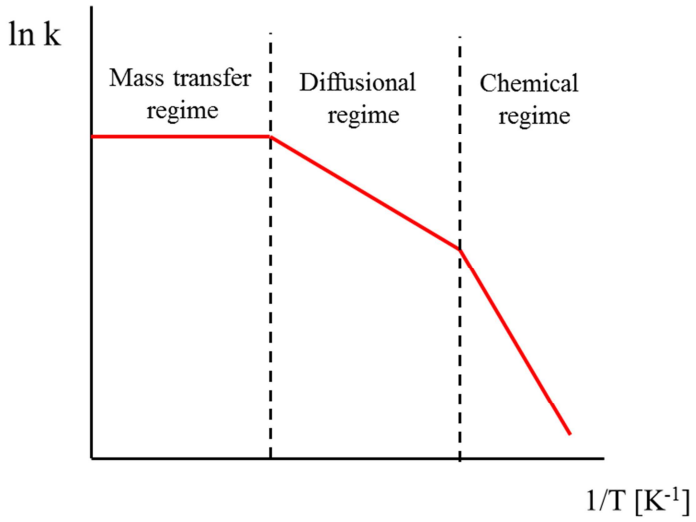

Figure 8: Illustration of the Arrhenius plot

Gas-solid reactions can always be expressed [21] by means of a chemical kinetic term, $f(T, Pi)$, accounting for temperature and reactant partial pressure effects, and a structural term, $g\ (X_i)$, implicitly or explicitly assumed to describe the effects of available internal surface .

$$r_c' = f\left(k_i, p_{H_2O}\right) g(X_c) \frac{dX_c}{dt} \qquad (12)$$

The latter observable reaction rate, Eq.12, for the heterogeneous steam gasification reaction will be scrutinized in the following chapters concerning the theory of structural effects and reaction mechanisms.

4.1.1 Structural models for the bagasse char particle

There are two widely applied concepts in modeling of non-catalytic gas-solid reactions: The progressive-conversion model (PCM) and the shrinking unreacted core model (SCM). The PCM and SCM models represent two idealizations that mark the extremes with respect to the reaction behavior of a solid particle and delimit the burn-off characteristics of real particle reacting with a surrounding fluid [20].

Lately, a significant effort has been put to model parameters to describe the internal solid matrix (grain model distribution) and its modification taking place during the char conversion [21], which represents more closely the reality.

Progressive-conversion model

The progressive-conversion model assumes that the diffusion rates in the gas and solid phase are very fast compared to the reaction rate. The concentration of the gaseous reactant inside the particle is everywhere the same and the overall gas-solid reaction rate is controlled by the intrinsic reactivity of the solid. While the reaction goes to completion, the solid particle is uniformly converted to solid and/or fluid products, but the particle size rests unaltered as the reaction goes to completion as it can be seen in the Figure 9.

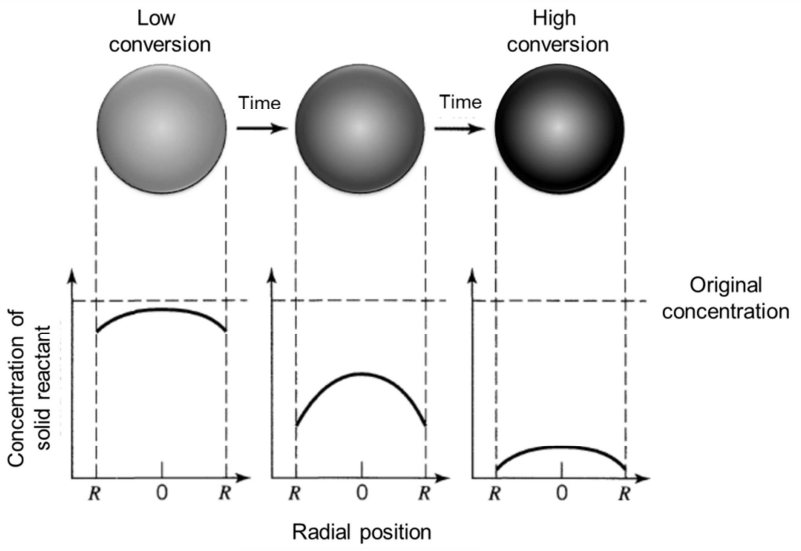

Figure 9: Progessive conversion model. [20].

Shrinking unreacted core model.

The shrinking core model (SCM) applies to non-porous particles and situations where the rate of reaction is fast compared to the diffusion rate in the solid. The reaction occurs at the outer skin of the unreacted particle. The reaction zone has the form of a sharp line moving into the solid and leaving behind completely converted as well as inert material, we refer to these as “ash”.

Two cases are possible:

(1) Shrinking spherical particles: No inert material is present and the solid is converted to a gas without the formation of residues. When chemical reaction controls, the behavior is identical to that particles unchanged size.

(2) Spherical particles of unchanged size: For materials with a high content of inert material, a solid ash layer is formed inhibiting further conversion due to diffusion limitation inside the particle.

(a) (b)

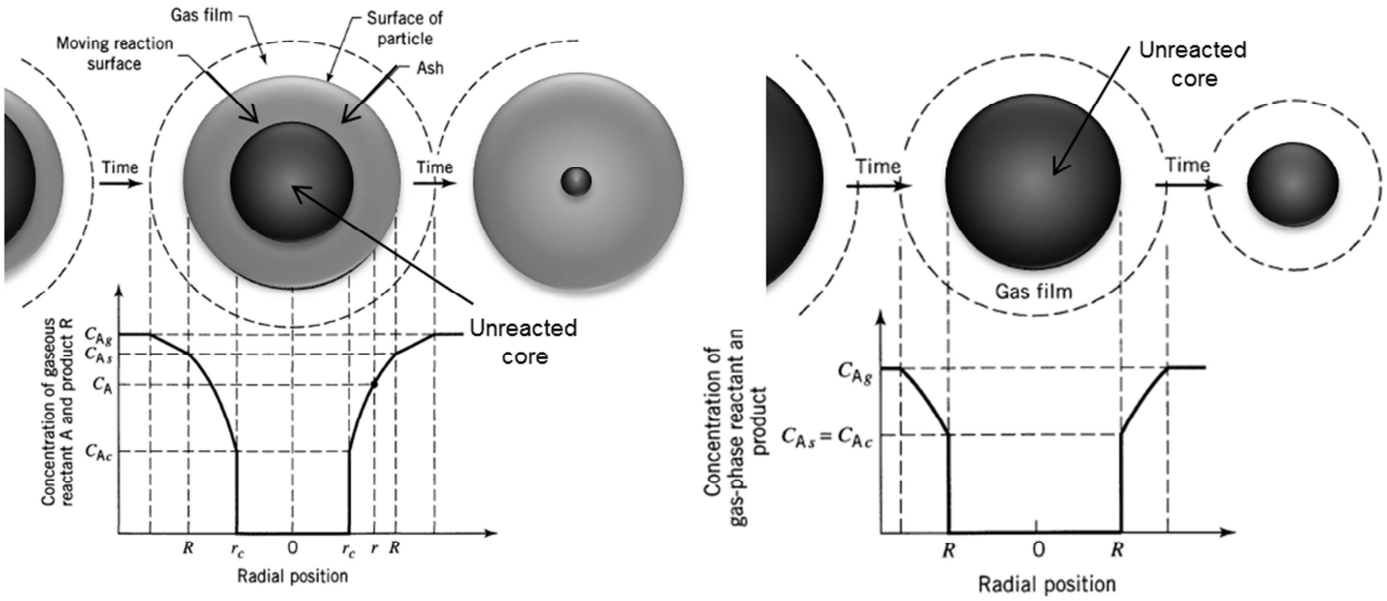

Figure 10: Representation of the reacting particle. (a) Constant particle size: all the stages can be controlling resistance. (b) Shrinking particles: Gas film diffusion controls. [20]

It is possible to extend the treatment also for non-spherical particles and for situations where combined effect of resistances must be considered.

A summary of the equations describing the aforementioned models is encountered in Table 5.

Table 5: Conversion-time expressions for various shapes of particles. Shrinking unreacted core model

		Film diffusion controls	Ash diffusion controls	Reaction controls
Constant size particle	Flat plate	$\frac{t}{\tau} = X$	$\frac{t}{\tau} = X^2$	$\frac{t}{\tau} = X$
	Cylinder	$\frac{t}{\tau} = X$	$\frac{t}{\tau} = X + (1-X)\ln(1-X)$	$\frac{t}{\tau} = 1 - (1-X)^{\frac{1}{2}}$
	Sphere	$\frac{t}{\tau} = X$	$\frac{t}{\tau} = 1 - 3\,(1-X)^{\frac{2}{3}} + 2\,(1-X)$	$\frac{t}{\tau} = 1 - (1-X)^{\frac{1}{3}}$

Shrinking sphere	Small particles	$\frac{t}{\tau} = 1 - (1 - X)^{\frac{2}{3}}$	Not applicable	$\frac{t}{\tau} = 1 - (1 - X)^{\frac{1}{3}}$
	Large particles	$\frac{t}{\tau} = 1 - (1 - X)^{\frac{1}{2}}$	Not applicable	$\frac{t}{\tau} = 1 - (1 - X)^{\frac{1}{3}}$

Grain model

The basic assumption of the grain model is that the solid behaves like an agglomeration of smaller units, the so called grains. Figure 11 (a) is a schematic of generic bagasse char particle considered as an agglomeration of smaller, randomly shaped grains. The individual grains are modeled as non-porous spheres of uniform sizes (Figure 11 (b)) each of which reacts with the surrounding accordingly with shrinking core model (Figure 11 (c)).

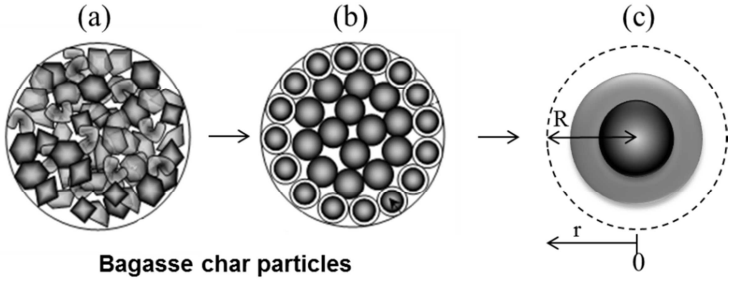

Figure 11: Schematic of the grain model. (a) Bagasse char particles are assumed to be an agglomeration of smaller grains. (b) Grains are modeled as spheres. (c) Each of them reacts individually with the surroundings (SCM).

The heterogeneous char gasification reaction taking place at the external surface of a single grain unit can be defined as follows:

$$r_c = -\frac{1}{s_{grain}} \frac{dN_c}{dt} \tag{13}$$

For a spherical grain, its surface area can be represented as:

$$s_{grain} = 4\pi r^2 \tag{14}$$

The carbon conversion, Xc, of a single grain depend on the grain radius.

$$X_c = \frac{N_{c,0} - N_c(t)}{N_{c,0}} = 1 - \left(\frac{r}{R}\right)^3 \quad (15)$$

Rearranging Eq. 15 to isolate radius, the structural term can be expressed in function of the conversion

$$s_{grain} = 4\pi r R^2 (1 - X_c)^{\frac{2}{3}} \quad (16)$$

And therefore, assuming SCM behavior, the gas-solid gasification reaction taking place at the external surface of the bagasse char particle becomes

$$r_c = -\frac{1}{s_{grain}} \frac{dN_c}{dt} = \frac{N_{c,0}}{S_0 (1 - X_c)^{\frac{2}{3}}} \frac{dX_c}{dt} \quad (17)$$

Where s_0 is the initial surface area available when $Xc = 0$ (extend of conversion) and 2/3 is the apparent reaction order.

Grain model distribution

This model presumes the porous particle to be a collection of grains of various sizes. And therefore, the special case where in which the original grains forming a particle have uniform size is not applicable, because in real life they consist of a mixture of different size grains. Small grains react faster while large ones are slowly converted.

Kimura et al. [22] proposed a model where the mean conversion rate of the particles is considered to have different dependence on the solid reactant in accordance with the magnitude of the variance of particle size distribution

Assuming the resistance to product layer diffusion in the grain is neglected, the concentration of the reactant throughout the particle is constant. And the progress of reaction in the grain is

$$\frac{t}{\tau} = 1 - (1 - X_c)^{\frac{1}{3}} \quad (18)$$

Where τ is the time required to complete the conversion of a grain. Then using a density function of the size distribution f(τ), the average conversion of the particle can be represented,

$$\overline{X_c} = \int_0^t f(\tau)\, d\tau + \int_t^\infty X_c\, f(\tau)\, d\tau \quad (19)$$

Being f(τ) a log-normal distribution expressed as,

$$f(\tau) = \frac{1}{\sqrt{2\pi}\sigma}\,\frac{1}{\tau}\; exp\left[-\left(\ln\frac{\tau}{\bar{\tau}}\right)^2 / 2\sigma^2\;\right] \tag{20}$$

Kimura et al. could develop a relation to the rate of conversion depending on the standard deviation and the unconverted solid. This relation was made using dimensionless parameters.

$$\frac{d\overline{X_c}}{d\theta} = \frac{3}{\sqrt{2\pi}}\exp\left(\frac{\sigma^2}{2}\right)\int_{\ln(\theta/\sigma)}^{\infty}(1-\theta\exp(-\sigma\varepsilon))^2\exp\left[-\frac{(\varepsilon+\sigma)^2}{2}\right]d\varepsilon \tag{21}$$

Where $d\overline{X_c}$ is the average conversion of the particle, θ is the dimensionless time t/τ and $\varepsilon = \ln(\tau/\bar{\tau})/\sigma$.

As the average conversion $\overline{X_c}$ is function of $f(\tau)$, it is obviously that it also depends on the standard deviation σ. Therefore, to better visualize the dependence of the reaction rate of the solid, the rate of conversion (Eq. 21) was plotted against the unconverted solid, $1 - X_c$.

The rate of conversion may be correlated with the unconverted solid by a straight line for each value of σ up to $\sigma = 1$. This suggested that a power law expression is suitable to represent the rate of conversion as follows,

$$\frac{d\overline{X_c}}{d\theta} = 3\exp\left(\frac{\sigma^2}{2}\right)(1-\overline{X_c})^m \tag{22}$$

Where m is the apparent reaction rate order with reference to the solid. From Eq. 22, it may be possible to understand that m varies accordingly to σ.

In fact, when $\sigma = 0$ where no deviation occurs, $m = 2/3$, and we come back to the grain model neglecting diffusional effects. When the standard deviation is around $\sigma = 0.5$, the apparent reaction appears to be $m = 1$, the same order as if the reaction would behave as homogeneous one and if the solid would not have influence.

This can be explained by two different approaches, either the grain voids created by pyrolysis are so big, that reactants can freely enter and react within the particle neglecting the existence of a neighboring surface, or there is a compensation in rate of consumption between the small and large grains that considering an overall effect, the outcome will be an apparent order of $m = 1$, as the small particle reacts faster than the large one.

4.1.2 Reaction mechanism

The steam gasification of char takes place according to several steps as reported by Barrio et al.[23]. They also point out that compared with CO_2, H_2O gasification is more complicated because, in addition to the main gasifying agent, the effects of H_2, CO_2 and CO should also be taken into account, owing to the equilibrium of the water gas shift reaction.

In the present work one mechanism is considered for the gasification of char with steam, the so called "oxygen-exchange mechanism" firstly suggested by Ergun [24]. The oxygen-exchange mechanism postulates the following series of equations:

$$C\langle * \rangle + H_2O \xrightarrow{k_1} C\langle O \rangle + H_2 \quad (23.\text{ a})$$

$$C\langle O \rangle + H_2 \xrightarrow{k_{-1}} C\langle * \rangle + H_2O \quad (23.\text{ b})$$

$$C\langle O \rangle \xrightarrow{k_2} C\langle * \rangle + CO \quad (24)$$

(k_1, k_{-1}, k_2 are Arrhenius rate constants), $C\langle * \rangle$ represents an active carbon site and $C\langle O \rangle$ a carbon-oxygen complex. The oxygen-exchange mechanism consists of Eq. 23-24 . Eq. 24 takes place at higher temperatures through the combination of oxygen and carbon atoms at the surface of the solid to form CO in gas phase. The latter normally controls the movement towards the equilibrium; therefore it may be taken as the rate determining step (rds).

The inhibition occurs by recombination of adsorbed oxygen with H_2. The dissociative chemisorption of H_2 on the active sites occurs and in this way the active sites become not accessible for the oxygen transfer with steam.

Assuming elementary reactions, their rates can be directly derived from their reaction expressions, as functions of their partial pressure in the bulk phase and the fractions of total number of sites that are vacant, or occupied by the reactants/products, θ_* θ_O:

$$r_{H_2O} = -k_1 N_T p_{H_2O} \theta_* + k_{-1} N_T p_{H_2} \theta_O \quad (25)$$

$$r_{H_2} = k_1 N_T p_{H_2O} \theta_* - k_{-1} N_T p_{H_2} \theta_O \quad (26)$$

$$r_{CO} = k_2 N_T \theta_O \quad (27)$$

N_T represents the total concentration of active sites. Conservation of total number of sites leads to the site balance expression:

$$1 = \theta_O + \theta_* \quad (28)$$

Under steady-state conditions, it can be considered sorption equilibrium, i.e, the concentrations of the vacant sites do not change in time,

$$\frac{d\theta_O}{dt} = k_1 p_{H_2O}\theta_* - k_{-1} p_{H_2}\theta_O - k_2\theta_O = 0 \quad (29)$$

From Eq. (24-25), the unknowns θ_O , θ_* can be expressed as functions of the rate constants and partial pressures, resulting:

$$\theta_O = \frac{k_1 p_{H_2O}}{k_1 p_{H_2O} + k_{-1} p_{H_2} + k_2} \quad (30)$$

For steady state conditions the rate of each reaction step equals the overall rate r_C. The fraction of surface covered with adsorbed oxygen is then substituted in the overall net rate equation, and dividing by k_2 gives the final rate law

$$r_C = k_2\theta_O = \frac{k_1 p_{H_2O}}{1 + \frac{k_1}{k_2} p_{H_2O} + \frac{k_{-1}}{k_2} p_{H_2}} \quad (31)$$

However, during the TG experiments, the gaseous products were constantly swept away from the reaction site, justifying the simplification $p_{H_2} = 0$. Thus, the gasification rate depends only on the steam partial pressure and temperature as follows

$$r_C = \frac{k_1 p_{H_2O}}{1 + \frac{k_1}{k_2} p_{H_2O}} \quad (32)$$

In order to describe the whole gas-solid reaction, Eq. 32 should be linked to the structural model described by Eq.12. The latter equation is dependent on the number of moles of char rate, and can be related to the char conversion X_c, with respect to the initial number of moles of char $N_{c,0}$ as

$$r_C = -\frac{1}{s_{grain}} \frac{dN_c}{dt} = \frac{N_{c,0}}{s_{grain}} \frac{dX_c}{dt} \quad (33)$$

The only information required to integrate Eq. 33 is the dependence of the effective char surface area on the char conversion $s_{grain} = s_{grain}(X_c)$. As aforementioned by the *"grain*

model distribution" the rate of char conversion may be correlated with the unconverted solid by a straight line for each value of σ up to $\sigma = 1$. This suggested that a power law expression is suitable to represent the effective surface area available with the progress of char conversion

$$s_{grain} = s_0 (1 - X_c)^m \tag{34}$$

Furthermore, Jovanovic [25] has demonstrated that for wide grain size distribution, a linear fit ($m = 1$) may be a reasonable approximation. Without trustful information about the effective grain size distribution of char particles, the latter was assumed as the initial guess. Combining Eqs. (32-34) with $m = 1$, the overall net gasification rate becomes,

$$r_C = \frac{k_1 p_{H_2O}}{1 + \frac{k_1}{k_2} p_{H_2O}} = \frac{N_{c,0}}{s_0} \frac{1}{1 - X_c} \frac{dX_c}{dt} \tag{35}$$

According to the fact that ash is present and ash-carbon structure is an unknown, the initial effective surface area participating in the gasification per mole of char remains also unknown. Thus, $S_0, N_{c,0}$ and r_c are lumped together into the apparent reaction rate r_c' with apparent rate constants k_1' and k_2' as follows

$$r_c' = r_C \frac{s_0}{N_{c,0}} = \frac{k_1' p_{H_2O}}{1 + \frac{k_1'}{k_2'} p_{H_2O}} = \frac{1}{1 - X_c} \frac{dX_c}{dt} \tag{36}$$

where,

$$k_i' = k_i \frac{s_0}{N_{c,0}} \tag{37}$$

Where k_1' and k_2' in Eq. 36 are described by means of Arrhenius parameters, pre-exponential factor k_0' and activation energy E_a.

4.2 Sample preparation and characterization

The bagasse passed through two different pyrolysis treatments before the steam gasification experiments. The slow pyrolysis, where the heating rate was maintained constant to 30 K/min and the rapid pyrolysis where the heating rate can reach up to 30'000 K/min.

The treatment conditions in pyrolysis determine the char yield and char reactivity. Those are important for the capacity of the gasifier. Reaching the lowest char yield and the highest char reactivity in pyrolysis is advantageous for gasification [26, 27]. It is believed that high heating rates result in less char formation but also more reactive in gasification. Therefore, in order to have more information about this behavior, bagasse was treated with high and low heating rates.

4.2.1 Sample preparation

The pre-treatments (slow and rapid pyrolysis) of bagasse samples were carried out in a laboratory-scale drop-tube fixed-bed pyrolyzer that was designed to simulate an indirectly heated solar-driven reactor. Figure 12 shows a schematic of the setup including the primary components and flows. The reactor consisted of a heat-resistant alumina tube (length 1'200 mm, inner diameter 60 mm, wall thickness 5 mm) that was placed inside an electrical tube furnace.

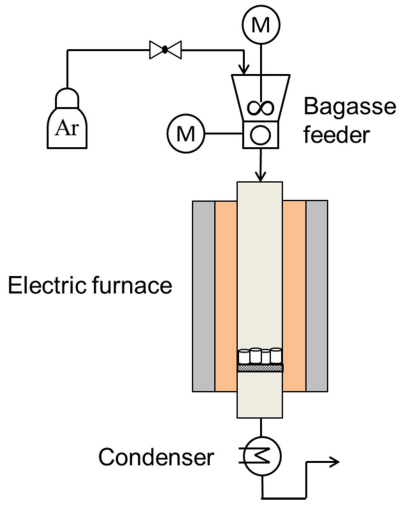

Figure 12: Schematic of the laboratory-scale biomass pyrolyser apparatus

A ceramic grate was placed at the hot zone of the tube to create a fixed bed where the char particles were collected. The flow rates of the inlet gases were controlled with electronic mass flow controllers (Bronkhorst). The product gas stream was cooled to remove condensable components and particulate matter [28].

Prior to each experiment, the reactor was purged with argon to remove oxygen in order to have an inert atmosphere.

Rapid pyrolysis

Both rapid and slow pyrolysis were performed in the electric furnace shown Figure 12. Empty ceramic pans were placed over a grade in the hot zone of the reactor in order to collect the reacted particles.

A screw feeder with a hopper filled with the dried bagasse was placed at the top of the reactor tube. Argon was injected into the hopper to prevent backflow of gaseous products into the feeding system.

After purging, 0.1 L_N/min[1] of argon was injected into the feeder and argon flow of 1 L_N/min was established inside of the reactor. The reactor was preheated to the desired temperature (1273 K). After 15 min of equilibration, bagasse was fed at an average rate of around 17 mg/s.

Finished the pyrolysis, the reactor was cooled down, and the pyrolyzed samples were removed from the reactor. Even if the pyrolyzed sample theoretically became hydrophobic, they were placed in an oven at 376 K, and kept there until the steam gasification experiment.

Slow pyrolysis

Ceramic pans were full filled with dried bagasse and placed over a grade inside of the reactor hot zone. The reactor was closed and after the purge, argon flow of 1 L_N/min was established.

[1] standard pressure and temperature

The reactor started to be heated up from 298 K with a constant heating rate of 30 K/min until 1273 K.

Finished the pyrolysis reaction, in both cases (rapid and slow pyrolysis), the reactor was cooled down, and the pyrolyzed samples were removed from the reactor. The same procedure as rapid pyrolysis pos-treatment was kept.

4.2.2 Bagasse char characterization

The composition of slow and rapid-pyrolyzed bagasse are also expressed in terms of ultimate analyses. Data analyses are shown in Table 6.

Table 6: Ultimate analysis of bagasse char (dry basis); C, H, N determined with CHN-900, O with RO-478 and S with CHNS-932 (all LECO Corporation, St. Joseph, MI)

		Rapid pyrolyzed char	Slow pyrolyzed char
Carbon (C)	[$\%_{wt}$]	29.50	46.72
Hydrogen (H)	[$\%_{wt}$]	0.60	0.10
Oxygen (O)	[$\%_{wt}$]	5.53	5.96
Nitrogen (N)	[$\%_{wt}$]	0.17	0.43
Sulfur (S)	[$\%_{wt}$]	0.12	0.11
Ash	[$\%_{wt}$]	64.08	46.70

With the information of ash content of both slow and rapid-pyrolyzed bagasse from the ultimate analysis and their remaining volatile content after the pyrolysis realized in the electric furnace setup, it was possible to calculate their char yield and total volatile production under different treatment conditions in pyrolysis. This information is listed in Table 7.

Table 7: Char yield for different treatments, rapid and slow pyrolysis (dry and ash free basis)

		Rapid pyrolyzed char	Slow pyrolyzed char
Volatiles	[%wt]	93.71	90.16
Fixed carbon	[%wt]	6.28	9.84

One can see from the table above that rapid pyrolysis produces less char than slow pyrolysis

Morphology

Figure 13 (a) and (b) shows a scanning electron micrograph (SEM) of bagasse char particles which undertook slow pyrolysis, magnified 600 and 1000 times. At the former magnification, pores are deceptively recognized, but at the latter magnification, it is possible to observe that the surface of the particle is pretty flat, having very little porous, which is expected to decrease the reactivity in the gasification

Figure 13 (c) and (d) shows a scanning electron micrograph (SEM) of bagasse char particles which undertook rapid pyrolysis, magnified 600 and 1000 times. From both magnifications it is possible to observe that rapid char particles have higher porosity compared to the ones in Figure 13 (a) and (b). These particles have low surface area, seen from the Table 8, and a non-uniform porous structure with a large central void surrounded by a thin shell. These macro-porous facilitate the reactants to reach the inner part of the grains and in consequence the reactivity in gasification is increased.

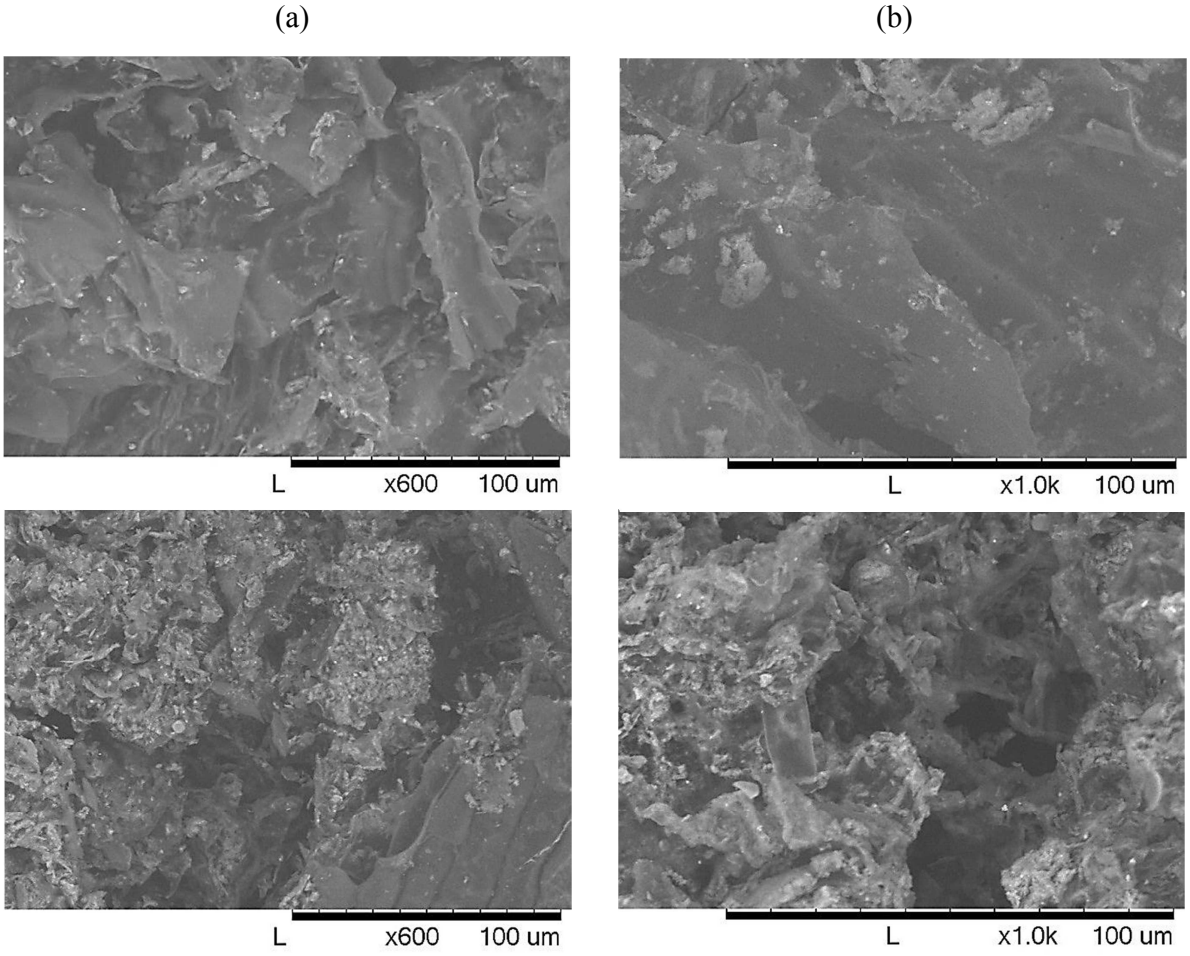

Figure 13: SEM micrographs of bagasse char particles. (a) and (b) bagasse particle that suffered slow pyrolysis 600 and 1000 times magnified respectively, (c) and (d) bagasse particles that suffered rapid pyrolysis 600 and 1000 times magnified respectively

Table 8: BET surface area report

	Bagasse	Rapid pyrolysed char	Slow pyrolysed char
BET surface area [m^2/g]	6.70 ± 0.17	20.40 ± 0.04	159.62 ± 2.08

4.3 Thermogravimetric analysis

The experiments in this chapter were performed with a thermogravimeter system (Netzsch STA 409 CD) equipped with special electric furnace with a maximum working temperature of 1523 K, suitable for reactive atmospheres containing up to 100% steam at 1 bar total pressure. A schematic of the steam-furnace with the main components indicated is shown in Figure 14 . The steam furnace is mounted on a double hoist system allowing alternative use and offering maximum flexibility with respect to experimental conditions such as temperature and steam concentration.

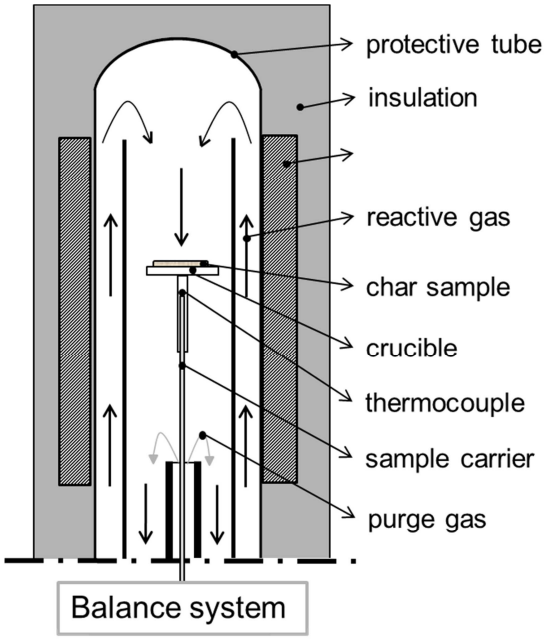

Figure 14: Cross-sectional schematics of the Netzsch steam furnace

The steam furnace (Figure 14) is used for the gasification runs with H_2O-Ar mixtures. The reactive gas enters the furnace chamber at the top end and flows downwards trough the char bagasse sample. The mixing of reactive gas (steam) and purge gas from the balance takes place near the exit of the furnace, offering the possibility to perform experiments with arbitrary steam concentrations up to 100%.

The steam furnace is coupled with a steam generator unit (Bronkhorst Hitec CEM) via a transfer line heated to 150°C to avoid the condensation of steam. Mechanical flow controllers for

Ar (Vögtlin Q-FLOW) and electronic flow controllers for water (Bronkhorst LIQUI-FLOW) are used to set the mass flow rates and the steam concentration in the reactive gas.

The experimental procedure of a gasification experiment with steam is rather similar to the pyrolysis run described in Chapter 3.2. The main difference is that experiments with the steam furnace have a bigger cycle time and are complicated by the operation of the steam generator and additional heaters that take longer to reach thermal equilibrium.

For the latter reason a special temperature program was used. Primarily, as usual, a “dynamic” pre-heating of the system is done with a constant heating rate of 30 K/min from room temperature to the desired temperature of gasification. Before reaching the starting point of gasification, the heating rate was gradually decreased from 30 to 1 K/min to reach faster the thermal equilibrium and avoid temperature overshooting. As soon as the thermobalance finished the automatic preheating sequence and equilibration, the steam valve was opened manually to feed the reactant to the furnace. The temperature is then kept constant and instantaneously the gasification reaction starts to take place. Isothermal data are thus used to evaluate the reaction kinetics.

The steam flow was controlled by a temperature safety valve and started to be generated only when the furnace reached a minimum temperature of 423 K.

To eliminate the buoyancy effect, all the experiments were repeated with the empty crucible (correction) and a baseline was thus obtained for the TG–DTG analysis. Prior to all experiments the crucible was oven dried in order not to have humidity of the air condensed over the pan where the dried sample laid.

Since the off-gas contained a considerable amount of water depending on the chosen composition of the reactive gas, a cooler was used after the thermobalance to condensate excess steam. This had to be done to protect the micro GC from contamination with liquid water. The water concentration in the off-gas could therefore not be measured.

The experiments of steam gasification were designed in the nearest way possible to what will occur inside of the solar reactor in order to take advantage of the kinetic data here simulated. Rapid and slow-pyrolyzed char were tested. Both experiments were carried out at a steam

concentration of 75%-vol in the temperature range 1173-1473 K. To assess the dependency on reactant concentration further experimental data just with rapid-pyrolyzed bagasse was collected at steam concentrations between 25 to 75%-vol at a temperature of 1273 K.

A list of all steam gasification runs and respective temperature and reactant concentration data is presented in Table 9

Table 9: Reactive gasification runs in the steam furnace with the corresponding experimental parameters.

Char type	m_0 (mg)	T_0,HR,T_{iso} (K,K/min,K)	purge	Reactive gas	
			F_{Ar} (mL_N/min)	F_{Ar} (mL_N/min)	Steam (%)
Rapid pyrolyzed bagasse	10.66	423/30/1173	132	25	75
	10.32	423/30/1223	132	25	75
	10.34	423/30/1273	132	25	75
	10.88	423/30/1373	132	25	75
	10.52	423/30/1473	132	25	75
	10.21	423/30/1273	132	75	25
	10.57	423/30/1273	132	50	50
Slow pyrolyzed bagasse	7.50	423/30/1173	132	25	75
	7.43	423/30/1273	132	25	75
	7.43	423/30/1373	132	25	75
	7.20	423/30/1473	132	25	75

4.4 Results and discussion

The experimental runs of steam gasification were performed with char particles produced via rapid pyrolysis and slow pyrolysis carried out in the electric furnace. The steam gasification was done in a steam furnace themogravimeter in order to compute the mass loss in time, necessarily to determine the kinetic rate law of bagasse char gas gasification. The sample was heated up until the desired temperature. The weight loss during this initial phase is mainly due to the evolution of remaining volatiles. After the pyrolysis, bagasse char particles are subjected to a mixture of reactive gas containing different proportions of argon and steam, shown in Table 9.

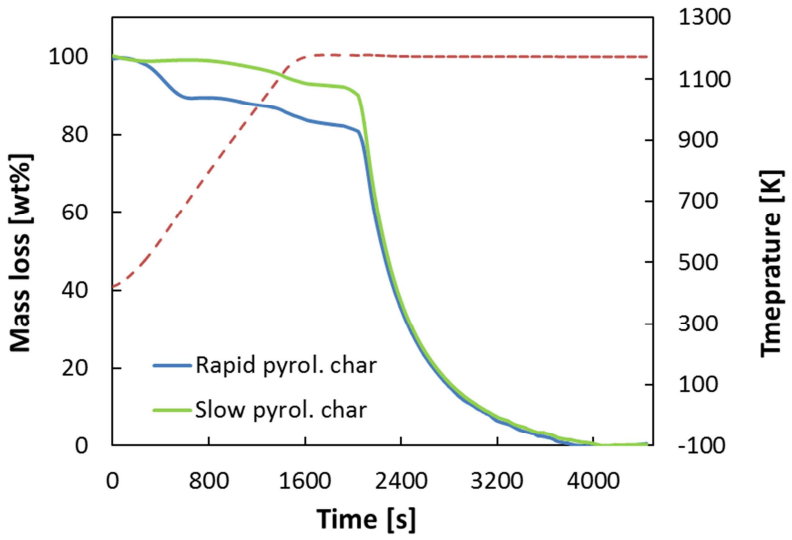

Figure 15: TG and data for steam gasification of rapid and slow pyrolyzed bagasse at T_{iso} = 1173 K with gasifying agent: 75%-vol/Ar mixture.

The typical TG curves obtained for the steam gasification of the slow and rapid-pyrolyzed bagasse are shown in Figure 15 as an example for the isothermal run with temperature of 1173 K and 75% of steam concentration. The latter figure represents the mass loss during the reaction, and it is reported as normalized dry and ash free basis for better comparison.

Figure 15 can be separated in two regions: the heating up, and the steam gasification itself. The visible weight loss of the rapid-pyrolyzed bagasse during the former is due to the occurrence of second pyrolysis step, probably because the time that those particles spent in the electric furnace hot zone was not enough to completely devolatilize them. Right before the steam gasification takes place, one can see a second weight loss, occurred for both samples. This could

be explained by a probable leaking of oxygen inside of the steam furnace, originating a slightly consumption of the solids by combustion. Steam was fed to the furnace after the equilibration of the desired temperature was reached; instantaneously the steam gasification started and converted the char into gases, leaving behind just an inert material called ash.

These experiments were used for modeling the steam gasification rate of reaction accounting for a structural and a kinetic term dependent on temperature and reactants partial pressure.

4.4.1 Structural term

The structural term of the steam gasification rate law was modeled by the grain model. The possibility of particles being represented as either spheres or flat plate and cylinder, as well as if film diffusion, ash layer diffusion or reaction at the surface controlled the process was investigated.

The assumption of having solid particles constituted of an agglomeration of smaller uniform units called grains that behave as non-porous particles and reacts individually with its surrounding following shrinking-core model (SCM) was kept as fundamental consideration.

In order to fit the equations from Table 5 to the experimental data collected by the thermogravimetric runs a least square routine was done my minimizing the parameters τ and Δt. τ is the time required for the full conversion of the char particles and Δt is the time elapsed to reach the experimental starting point of the char conversion X_c, since this did not began from a time zero. Two minimization methods were used. Either the fit was minimized in t or in X_c direction,

$$\sum\left[(X.\tau + \Delta t) - t_{exp}\right]^2 \qquad \sum\left[\frac{t-\Delta t}{\tau} - X_{c\,exp}\right]^2 \tag{38}$$

Figure 16 illustratively shows the experimentally measured and modeled conversion of rapid pyrolyzed bagasse during the steam gasification in conditions of 1273 K and 75%-vol steam/Ar for two different cases commented above: reaction controls, and ash layer diffusion controls.

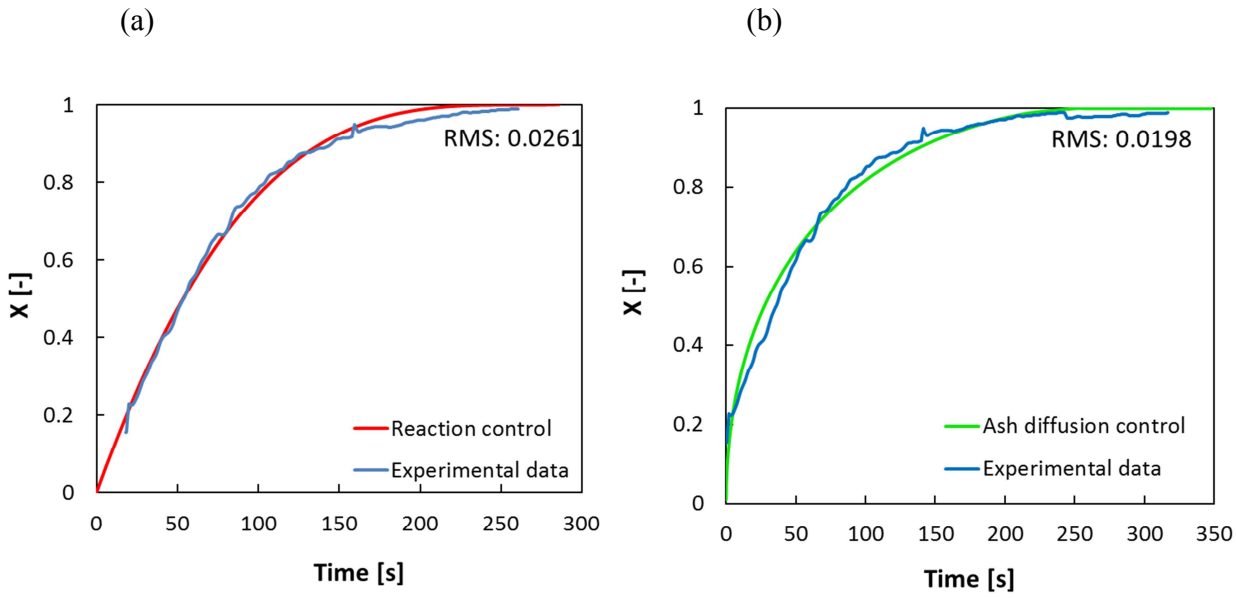

Figure 16: Experimentally measured and modeled conversion of rapid char shaped sphere assuming the rds to be the surface reaction (a) and conversion of char shaped sphere assuming the rds to be the ash layer diffusion (b). Both runs are undertaken at 1273 K with gasifying agent: 75%-vol steam/Ar mixture.

Numerical models with all the equations listed in Table 5 were attempted to fit both rapid and slow-pyrolized bagasse steam gasification reactions. However the agreement was not reasonable. Therefore the assumption of having grains of uniform sizes was not valid for this series of experiments.

One may assume that the solid contains enough voidage to let pass freely the fluid reactant or product and that the solid grains are distributed homogeneously throughout the solid phase. Wen [19] stated that may be reasonable to consider that reactions between fluid and solid are occurring in homogeneously ($m = 1$) throughout the solid phase.

On the other hand Kimura et al. [22] suggests a power law expression (Eq. 22) to represent the conversion of particles consisted of grains with a distribution of sizes, this model is called *"grain model distribution"*. The latter model was not applied to the experiments since no trustful information about the effective grain size distribution of char particles were known. Nevertheless Jovanovic [25] has demonstrated that for wide grain size distribution, a linear fit ($m = 1$) may be a reasonable approximation.

Figure 17 shows the experimentally measured and numerically modeled conversion of rapid-pyrolyzed bagasse in the same conditions of Figure 16 for the linear model.

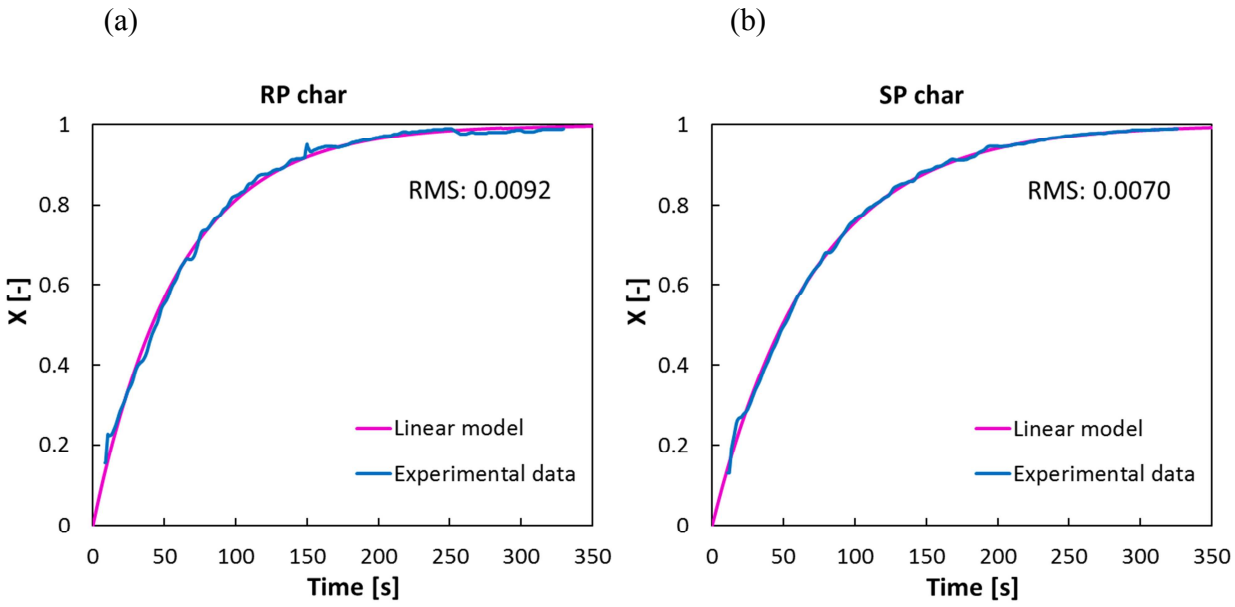

Figure 17: Experimentally measured and modeled by the linear model conversion of (RP) rapid char (a), (SP) slow char (b). Runs undertaken at 1273K and with gasifying agent: 75%-vol steam/Ar mixture.

Indeed the agreement is very good for the conversion of the rapid-pyrolyzed bagasse and excellent for the slow-pyrolyzed char during the steam gasification, as the RMS obtained were in both cases the minimum. From now on, the structural term $g(X_c)$ in Eq.12 is then represented by the linear model (Eq.39), meaning that the apparent order of reaction rate is equal to $m = 1$. This could be applied successfully for both bagasse chars.

$$r_c' = f\left(k_i, p_{H_2O}\right)(1 - X_c)^1 \frac{dX_c}{dt} \quad (39)$$

4.4.2 Kinetic term

Lastly, what is missing to complete the evaluation of the steam gasification rate of reaction is the kinetic term, which depends on temperature and partial pressure of the reactants.

The temperature dependence is expressed by the activation energy, E_a, and pre-exponential factor, k_0, of the apparent constant rate as it follows Arrhenius law a. By the least square routine applied before, for each experiment with a different T_{iso}, it was possible to calculate their reaction rate constants. Figure 18 illustrates the linearized Arrhenius plot and the experimental determined apparent rate constants.

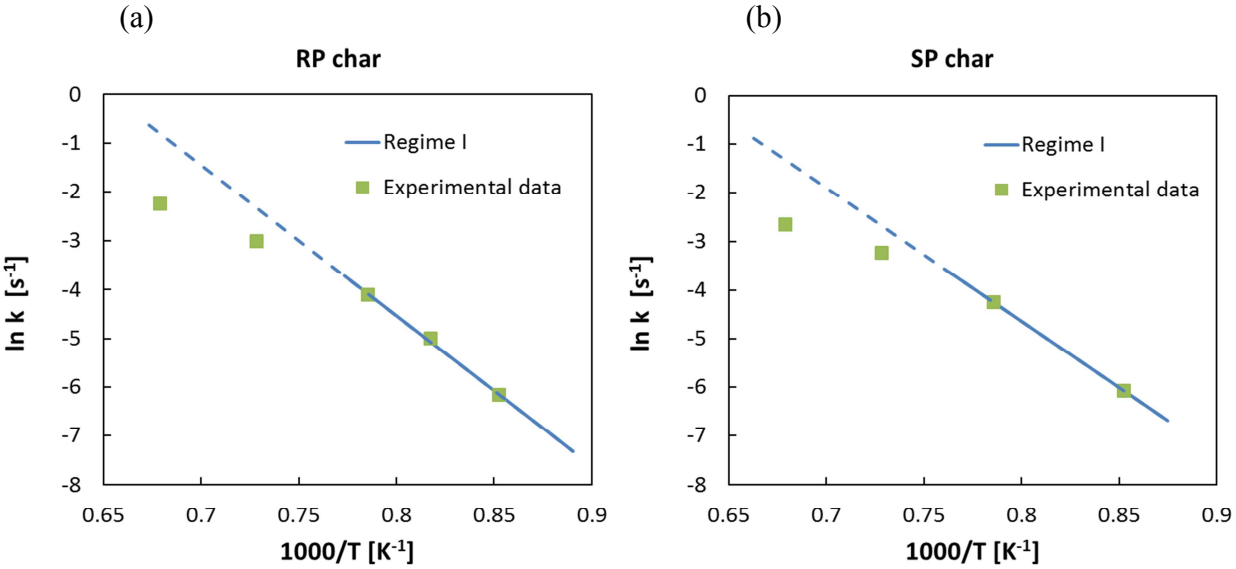

Figure 18: Experimentally determined and modeled reaction rate constants for (RP) rapid char (a), and (SP) slow char (b). Runs in the range of 1173 to 1473 K and with gasifying agent: 75%-vol steam/Ar mixture.

Considering a linear contribution for the reactant partial pressure, the Arrhenius plot (Figure 18) shows that the rate constants are in agreement with the model for low temperatures.

Comparing the latter figure with Figure 8 it is possible to claim that for temperatures up to 1273 K the regime controlling the reaction is the reaction at the surface (Regime I). However, when increasing the temperature, the slope of the experimental data decreases and deviates from Regime I. Thus the reaction appears to be influenced by diffusional effects. Accordingly to O. Levenspiel [20], for catalytic solid reactions, if the curve slope is half of the value of the curve slope at chemical controlling regime, strong pore resistance exists.

In any case, for the present analysis diffusion limitation was neglected since the deviation reported in Figure 18 was not enough to make decisive conclusions. Besides, we are performing non-catalytic solid reactions. Therefore, only data from Regime I was used to compute the kinetics parameters, activation energy, E_a, and pre-exponential factor, k_0.

Table 10: Arrhenius kinetic parameters for steam gasification reaction of rapid and slow-pyrolyzed bagasse

Char type	$k_0'[s^{-1}\ bar^{-1}]$	$E_a'\ [J/mol]$
Rapid-pyrolyzed bagasse	6.38E+08	2.56E+05
Slow-pyrolyzed bagasse	3.50e+07	2.27E+05

No kinetic data of steam gasification of bagasse char was encountered in literature to make a direct comparison. Cetin [8] studied the gasification of sugarcane bagasse char with CO_2 under isothermal conditions and found an activation energy value of 1.98E+05 J/mol. The steam gasification of other biomasses reported values between 1.96E+05-2.70E+05 J/mol [21]. Despite this vast range, it is possible to state that the values reported in the present work are in good agreement in relation to the activation energies of the biomass gasification reaction encountered in literature.

The reactant partial pressure dependency evaluated by the *"oxygen-exchange mechanism"* was applied just for the rapid-pyrolyzed bagasse steam gasification reaction.

In order to compute the kinetic parameters $k'_{0,i}$ and $E'_{a,i}$ from k'_i of Eq. 36, a least square fit of the integral form of the right hand side of the latter equation with the experimental data of rapid char conversion X_c was applied. Eq. 36 thus becomes,

$$r'_c = r_C \frac{s_0}{N_{C,0}} = \frac{k'_1 p_{H_2O}}{1+\frac{k'_1}{k'_2} p_{H_2O}} = -\frac{\ln(1-X_c)}{t} \qquad (40)$$

Figure 19 presents the employment of Eq. 40 against all the experiments carried with different T_{iso} in the range of 1173 – 1473 K with a gasifying agent of 75%-vol steam/Ar mixture.

(a) (b)

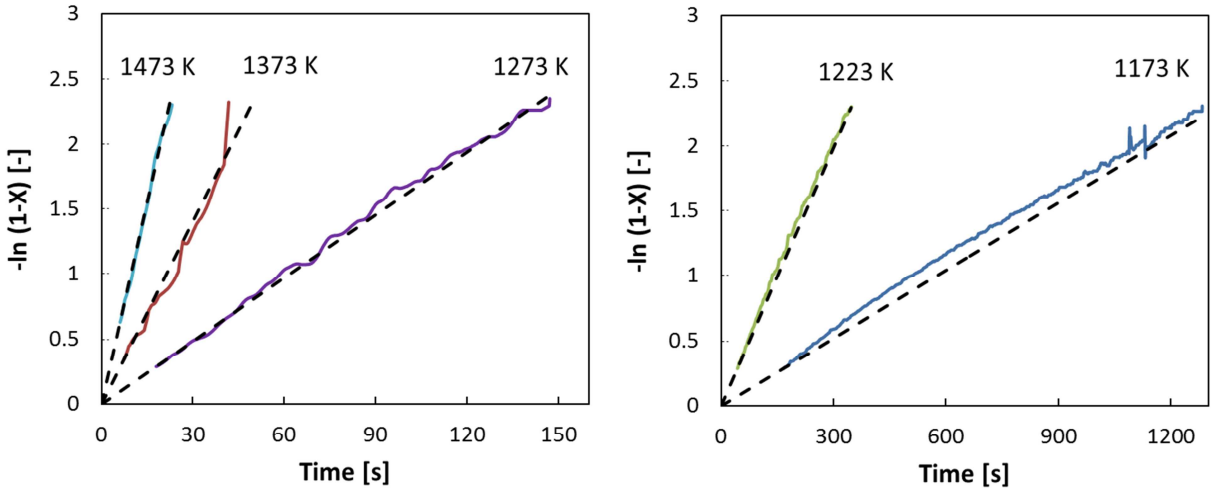

Figure 19: Experimentally and modeled $-ln(1-X_c)$ vs. $time$, for experiments at T_{iso} 1273-1473K (a) and T_{iso} 1173-1223K (b) . Runs with gasifying agent: 75%-vol steam/Ar mixture.

The reasonable linearity of the plots in Figure 19 justifies the use of a linear dependence of the structural term and allows the extraction of the experimental reaction rates as slopes of the fittings are straight lines. Those were then used to compute the apparent kinetic parameters for the rapid-pyrolyzed bagasse steam gasification reaction, which are listed in Table 11

.

Table 11: Arrhenius kinetic parameters of *"oxygen-exchange mechanism"* applied to steam gasification reaction of rapid pyrolysed bagasse

Kinetic parameters	$k_1'[s^{-1}\,bar^{-1}]$	$k_2'[s^{-1}]$
$k_0'\ (k_i')$	55.8	4.27E+11
$E_a'\ [J/mol]$	7.37E+04	3.21E+05

Oxygen-exchange mechanism, reported in literature as Langmuir-Hinschelwood kinetics is considered only in a few cases [21]. Some of them also considered the H_2-inhibition effect [23, 29], neglected in the present work because H_2 was constantly swept away from the reaction environment. Unfortunately no data of steam gasification of biomass that undertook the same conditions as in this present work was found to make comparison.

In order to evaluate the dependence of the reaction rate on the partial pressure of the reactant, experiments at temperature 1273K with a rage of gasifying agent varying from 25-75%-vol steam/Ar were done. In addition, having the rate constant values k_i', a nonlinear regression was done to describe the apparent reaction rate as a function of partial pressure. The dependency of the reaction rate on the partial pressure for the rapid-pyrolysed bagasse is shown in Figure 20.

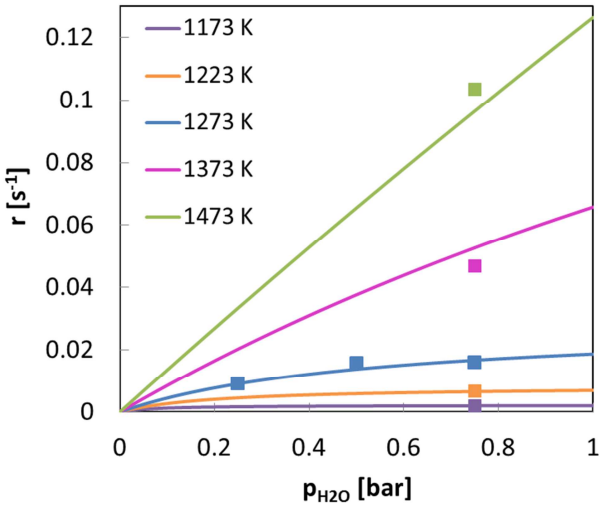

Figure 20: Steam gasification apparent reaction rate as a function of partial pressure for the steam gasification with different mixture of the gasifying agent.

The agreement of the curves is reasonably god with the experimental points at 1273 K. The behavior at other temperatures are included just to illustrate that the same treatment would be extensible to other temperatures, even if just one experimental point was produced.

In an overview of all the experiments done for the rapid-pyrolized bagasse and the employment of the "oxygen-exchange mechanism" one can see from Figure 21 that the apparent reaction modeled has a good parity with the experimental one, and demonstrates therefore reproducibility of results.

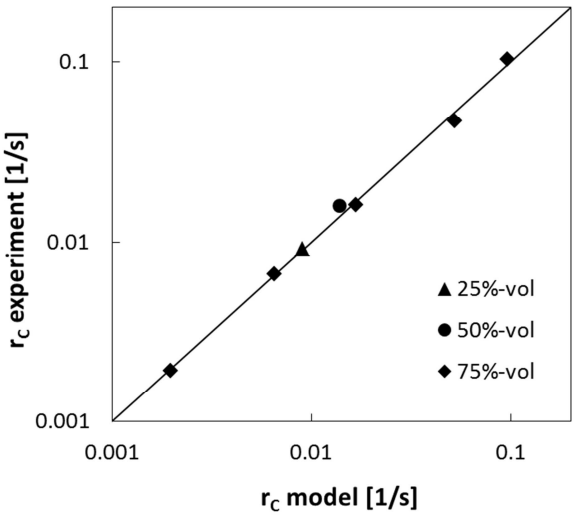

Figure 21: Apparent reaction rate for the experimental measurements vs. the model for the temperature range 1173-1473 K and 25-75 %-vol steam/Ar concentration.

5 Conclusions

The Brazilian sugarcane bagasse turned out to be a very promising feedstock for the solar-steam-gasification process, as it is very abundant by-product from the sugar industry and its current use is very inefficient.

The steam gasification process encloses two consecutive reactions: Pyrolysis and steam gasification. Both were experimentally studied by thermogravimetric analysis in order to model their rate laws, which are of fundamental importance for the design of the solar reactor.

The pyrolysis experiments were carried at from room temperature until 1473 K, with constant heating rates varying from 10-30 K/min.

Pyrolysis was successfully described as a linear combination of first order decomposition steps. Predictions from the model proposed here (contemplating three-pseudo-components) reproduce correctly the experimental TG curves during the pyrolysis of the bagasse in this study.

SEM images showed that chars produced by pyrolysis at high and slow heating rates have very different pore-structure and available surface area. This may have an impact on the reactivity in gasification.

The steam gasification of the slow and rapid-pyrolyzed bagasse were experimentally studied in the temperature range of 1173 – 1473 K, with a gasifying agent mixture steam/Ar of 75%-vol. In addition, the reactive gas composition was varied from 25-75% in experiments just with the rapid-pyrolized bagasse at 1273 K.

A linear correlation was introduced to describe the structural effect based on a broad distribution of effective particle size diameter. The structural term is well predicted as a linear dependence of the unconverted char for both slow and rapid-pyrolyzed bagasse.

Oxygen-exchange mechanism could describe well the behavior of the steam-gasification as it accounts for a reaction an adsorption terms in the surface. The oxygen-exchange mechanism

accounting for the temperature and partial pressure of the reactant represented the experiment result with a good agreement for the temperature range of the experiments.

References

1. Teixeira, F., *Bagaço de cana-de-açúcar na alimentação de bovinos.* Revista eletrónica de veterinária, 2007. **8**(6): p. 1695-1704.
2. Ulloa, C., A.L. Gordon, and X. García, *Distribution of activation energy model applied to the rapid pyrolysis of coal blends.* Journal of Analytical and Applied Pyrolysis, 2004. **71**(2): p. 465-483.
3. Piatkowski, N. and A. Steinfeld, *Reaction kinetics of the combined pyrolysis and steam-gasification of carbonaceous waste materials.* Fuel, 2010. **89**(5): p. 1133-1140.
4. Taylor, R.W., R. Berjoan, and J.P. Coutures, *SOLAR GASIFICATION OF CARBONACEOUS MATERIALS.* Solar Energy, 1983. **30**(6): p. 513-525.
5. Piatkowski, N., et al., *Solar-driven gasification of carbonaceous feedstock—a review.* Energy & Environmental Science, 2011. **4**(1): p. 73.
6. Stubington, J.F. and S. Aiman, *PYROLYSIS KINETICS OF BAGASSE AT HIGH HEATING RATES.* Energy & Fuels, 1994. **8**(1): p. 194-203.
7. Babu, B.V. and A.S. Chaurasia, *Pyrolysis of biomass: improved models for simultaneous kinetics and transport of heat, mass and momentum.* Energy Conversion and Management, 2004. **45**(9-10): p. 1297-1327.
8. Cetin, E., et al., *Biomass Gasification Kinetics: Influences of Pressure and Char Structure.* Combustion Science and Technology, 2005. **177**(4): p. 765-791.
9. Shen, J., et al., *Effects of particle size on the fast pyrolysis of oil mallee woody biomass.* Fuel, 2009. **88**(10): p. 1810-1817.
10. Garcia-Perez, M., et al., *Fast pyrolysis of oil mallee woody biomass: Effect of temperature on the yield and quality of pyrolysis products.* Industrial & Engineering Chemistry Research, 2008. **47**(6): p. 1846-1854.
11. Lakshmanan, C.C. and N. White, *A NEW DISTRIBUTED ACTIVATION-ENERGY MODEL USING WEIBULL DISTRIBUTION FOR THE REPRESENTATION OF COMPLEX KINETICS.* Energy & Fuels, 1994. **8**(6): p. 1158-1167.
12. Pitt, G.J., *THE KINETICS OF THE EVOLUTION OF VOLATILE PRODUCTS FROM COAL.* Fuel, 1962. **41**(3): p. 267-274.
13. Orfao, J.J.M., F.J.A. Antunes, and J.L. Figueiredo, *Pyrolysis kinetics of lignocellulosic materials - three independent reactions model.* Fuel, 1999. **78**(3): p. 349-358.
14. Gomez-Barea, A., P. Ollero, and R. Arjona, *Reaction-diffusion model of TGA gasification experiments for estimating diffusional effects.* Fuel, 2005. **84**(12-13): p. 1695-1704.
15. Ollero, P., et al., *Diffusional effects in TGA gasification experiments for kinetic determination.* Fuel, 2002. **81**(15): p. 1989-2000.

16. Varhegyi, G., et al., *KINETICS OF THE THERMAL-DECOMPOSITION OF CELLULOSE, HEMICELLULOSE, AND SUGAR-CANE BAGASSE.* Energy & Fuels, 1989. **3**(3): p. 329-335.

17. Roquediaz, P., et al., *STUDIES ON THERMAL-DECOMPOSITION AND COMBUSTION MECHANISM OF BAGASSE UNDER NON-ISOTHERMAL CONDITIONS.* Thermochimica Acta, 1985. **93**(SEP): p. 349-352.

18. Manya, J.J., E. Velo, and L. Puigjaner, *Kinetics of biomass pyrolysis: A reformulated three-parallel-reactions model.* Industrial & Engineering Chemistry Research, 2003. **42**(3): p. 434-441.

19. Ishida, M. and C.Y. Wen, *COMPARISON OF KINETIC AND DIFFUSIONAL MODELS FOR SOLID-GAS REACTIONS.* Aiche Journal, 1968. **14**(2): p. 311-&.

20. Levenspiel, O., *Chemical reaction engineering*. 3rd ed1999, New York: Wiley. 668.

21. Di Blasi, C., *Combustion and gasification rates of lignocellulosic chars.* Progress in Energy and Combustion Science, 2009. **35**(2): p. 121-140.

22. Kimura, S., S. Tone, and T. Otake, *Reaction order in the grain model with grain size distribution.* Chemical engineering of Japan, 1981. **14**(6): p. 491 - 493.

23. Barrio, M., et al., *Steam Gasification of Wood Char and the Effect of Hydrogen Inhibition on the Chemical Kinetics.* Progress in Thermochemical Biomass Conversion, 2008.

24. Ergun , S., *Kinetics of the reaction of carbon dioxide and steam with coke*1962: US Bur Mines Bull.

25. Jovanovic, Z.R., *Kinetics of direct nitridation of pelletized silicon grains in a fluidized bed: experiment, mechanism and modelling.* Journal of Materials Science, 1998. **33**(9): p. 2339-2355.

26. Liliedahl, T. and K. Sjostrom, *Modelling of char-gas reaction kinetics.* Fuel, 1997. **76**(1): p. 29-37.

27. Zanzi, R., K. Sjostrom, and E. Bjornbom, *Rapid pyrolysis of agricultural residues at high temperature.* Biomass & Bioenergy, 2002. **23**(5): p. 357-366.

28. Simell, P., et al., *Provisional protocol for the sampling and anlaysis of tar and particulates in the gas from large-scale biomass gasifiers. Version 1998.* Biomass & Bioenergy, 2000. **18**(1): p. 19-38.

29. Bjerle, I., et al., *THERMOGRAVIMETRIC ANALYSIS OF SWEDISH SHALE CHAR - KINETICS OF THE STEAM CARBON AND CARBON-DIOXIDE CARBON REACTIONS.* Industrial & Engineering Chemistry Process Design and Development, 1982. **21**(1): p. 141-149.

Nomenclature

E_a	Activation energy	[J/mol]
E_a'	Apparent activation energy	[J/mol]
k_i	Rate constant	[rate dependent]
k_i'	Apparent rate constant	[rate dependent]
$k_{0,i}$	Pre-exponential factor	[rate dependent]
$k_{0,i}'$	Apparent pre-exponential factor	[rate dependent]
X_T	Total bagasse conversion	[−]
X_c	Char conversion	[−]
$X_{c_{exp}}$	Char conversion	[−]
p_{H_2O}	Partial pressure of steam	[bar]
p_{H_2}	Partial pressure of hydrogen	[bar]
F_{Ar}	Volumetric flow of argon	[mL_N/min]
r_c	Rate of char conversion	[rate dependent]
r_c'	Apparent rate of char conversion	[rate dependent]
r	Radius of the char particle consumed in time	[m]
R	Initial radius of char particle	[m]
HR	Heating rate	[K/min]
HHV	High heat value	[MJ/kg]
LHV	Low heat value	[MJ/kg]

m_0	Initial mass	[mg]
m	Apparent reaction order	[−]
R	Ideal gas constant	[J/Kmol]
t	Time	[s]
t_{exp}	Experimental time	[s]
τ	Time for full conversion of the char particle	[s]
θ	Dimensionless time	[−]
Δt	Time elapsed to reach the experimental starting point	[s]
ΔH_R	Enthalpy of reaction	[KJ/mol]
σ	Standard deviation	[−]
$f(\tau)$	Log-normal distribution	[−]
T	Temperature	[K]
T_0	Initial temperature	[K]
T_{end}	Final temperature	[K]
T_{iso}	Isothermal temperature	[K]
N_c	Number of moles of char	[mol]
$N_{c,0}$	Initial number of moles of char	[mol]
s_{grain}	Surface area of a grain	[m^2]
s_0	Initial surface area of a grain	[m^2]
θ_O	Fraction of surface covered with oxygen	[−]
θ_*	Fraction of available surface	[−]

Abbreviation

SP	Rapid-pyrolyzed bagasse
RP	Slow-pyrolyzed bagasse
TG	Thermogravimetric analysis
DTG	Differential thermogravimetric analysis
SCM	Shrinking unreacted core model
PCM	Progressive conversion model
rds	Rate determining step
RMS	Root mean square
daf	Dry ash free basis
SEM	Scanning electron microscopy
BET	Brunauer - Emmett - Teller